Pure Appl. Chem., Vol. 74, No. 9, pp. 1631–1641, 2002.

Nonequilibrium processes for generating silicon nanostructures in single-crystalline silicon*

P. Sen[1,‡] and J. Akhtar[1,2]

[1]School of Physical Sciences, Jawaharlal Nehru University, New Delhi 110067, India; [2]Microelectronics Technology Group, Semiconductor Devices Area, CEERI, Pilani, Rajasthan 333031, India

Abstract: The possibility of modifying existing materials through technology has become the recipe for preparation of advanced materials. Nonequilibrium processing of silicon through MeV ion irradiation will be shown here to yield interesting properties. We propose localization of vibrational energy following an ion irradiation process and their transport (nonlinear transport of energy) through linear chains of a single-crystalline lattice. The localization of energy can involve 3–4 atoms, and, hence, nanometer-sized entities evolve, distinguishable from the remaining periodic lattice owing to their unique interatomic distances. The energy required to produce these structures is supplied by a single high-energy heavy ion, incident normal to a suitable crystal face so as to lose energy by the electronic energy loss mechanism. These entities can be trapped at a desired location that leads to silicon nanostructures with modified band-gaps.

INTRODUCTION

Currently, there is interest in how energy, supplied to a single-crystalline lattice in the way of energetic heavy ions, incident on a single crystal, is dispersed from the initial track. The region of interest is near the sample surface where the ions suffer slowing down as a result of electronic loss. The best systems to study transient disorder and their evolution are naturally those that are most widely understood. Silicon is such a system, where highly pure single crystals are available and further knowledge of MeV ion-induced processes is desired. There are various reports in the literature of defect production in Si, subjected to swift heavy ions.

In recent experiments, employing MeV ion irradiation to induce defects in Si single crystals, Levalois et al. [1] failed to observe any defect formation even with 3.6 GeV uranium [electronic energy loss, $S_e = (dE/dx)_e = 24$ keV/nm]. This was verified on the basis of transmission electron microscopy (TEM) studies. A similar observation [2] has been reported by Varichenko et al., employing 5.68 GeV Xe ions to induce irradiation effects in Si(111). The authors report formation of point defects at end-of-range, where nuclear stopping is operative, but amorphization or disorder are absent in regions where the ions lose energy through electronic means. These authors suggest that electronic stopping suppresses damage formation.

The situation is quite different for polycrystalline materials. In a detailed study, Furuno et al. made a comparative evaluation of thin films of Ge, Si, and Ti for various S_e values [3]. Tracks are reported in Si for S_e values in excess of 12 KeV/nm, and the track diameters for all these systems scaled with S_e. Also, based on values reported here of S_e-onset to track formation, the systems can be ordered

---

Pure Appl. Chem.* **74, 1489–1783 (2002). An issue of reviews and research papers based on lectures presented at the 2nd IUPAC Workshop on Advanced Materials (WAM II), Bangalore, India, 13–16 February 2002, on the theme of nanostructured advanced materials.

‡Corresponding author: E-mail: prasenjitsen@vsnl.net

in the following sequence Ge < Si < Ti, which is consistent with the general understanding that metals are less prone to radiation damage [4].

This raises the query as to why a material in its single crystalline form with inherent long-range order is resistant to radiation damage through S_e, although the initial coupling of the ion energy via electronic energy loss should not be affected substantially by lattice order in the immediate neighborhood of the irradiation site. Is there a global or long-range effect that transports the disorder or energy, or both?

MeV ions and the mechanism of energy loss

The MeV ions employed here settle fairly deep inside the lattice, losing energy in its path. Near the surface of the sample, where the ion enters, the energy loss mechanism is electronic in nature. The behavior of the energy loss with depth depends on the ion-substrate combination.

Electronic energy loss is a consequence of direct interaction of the incident ions with the target electrons. The incident ion, depending upon its velocity, either ionizes the target atoms or gets further ionized itself. Energy transferred to the electron in a direct collision is approximately 4 m_e E/M, where m_e and M refer to the mass of the electron and the incident ion, respectively. If the energy transferred to the electron is less than the ionization energy of the target atoms, energy loss to the electron is improbable. If I_t is the ionization potential of the target atom, to ionize it the projectile energy must exceed $E_{t1} = I_t M/4\ m_e$.

If I_t = ~10 eV, then E_{t1} is ~5 KeV for proton projectiles and ~ 200 KeV for Ar ions. Similarly, the threshold for the ionization of a projectile is given as $E_{t2} = I_p M/4\ m_e$, where I_p is the ionization potential of the projectile. For hydrogen atom, I_p = 13.6 eV and so E_{t2} ~ 7 KeV, i.e., above 7 KeV, bare protons will be the projectiles rather than hydrogen atoms. In case of Ar^+ ions, E_{t2} = 300 KeV. If the ion energy falls below this value, it will collect electrons and pass through the target as a neutral Ar atom.

Electronic loss would be significant when ion energy exceeds not only E_{t1} but also E_{t2}, as a neutral atom will ionize little even if its energy is above E_{t1}. The threshold for the onset of electronic energy loss is thus proportional to the mass of the incident ion. Once the ion energy is above the threshold, energy loss would depend largely upon the charge state of the incident ion.

Figure 1 shows the electronic energy loss suffered by 2 ions, namely, 100 MeV Ti^{7+} (lower plot) and 200 MeV Ag^{14+} (upper plot) in silicon, calculated employing transport of ions in matter (TRIM). It is seen that the Ti ion settles at a depth of about 20 μm, while the Ag ion settles at 24 μm. For Ag, the energy loss at the surface is 12.5 MeV/μm and decreases continuously until the end of range, while for Ti, the energy loss is constant over several microns inside silicon.

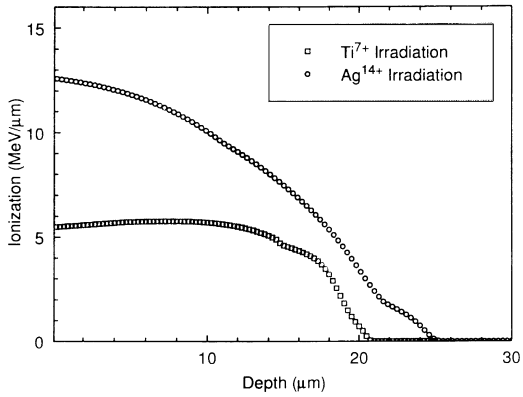

Fig. 1 TRIM ionization profiles of the 100 MeV Ti^{7+} (lower plot) and 200 MeV Ag^{14+} (upper plot) irradiated samples.

EXPERIMENTAL PROCEDURES

Creation of irradiation interfaces

We address the observation of lack of irradiation damage through MeV ion energy loss by employing an experimental procedure that would produce an irradiation interface, creating a "hot" region (or region under irradiation) on one side and a "cold" region next to it. In case the "cold" region is affected, one can provide evidence of MeV ion-induced modifications, at locations spatially separated from the region of ion impact with the lattice. A square grid composed of Ni wires, having square cross-section with 40-μm edge length, at a spacing of 850 μm, was placed between 5 mm to 20 cm in front of the (100) face of a Si single crystal.

The choice of the wires is important. They are polycrystalline, and the thickness is approximately double the range of the MeV ions employed. This prevents any possibility of channelling or transmission of 200 MeV silver ions through the wires. We considered the possibility of forward sputtering from the nickel grid onto the Si(100) crystal. But this would have been removed by the etching experiments discussed below.

Ion irradiation experiments

The ion irradiation experiments reported here were carried out by the NSC, New Delhi, using a 15UD Pelletron accelerator under a vacuum of 10^{-6} torr, at room temperature. The flux was kept low at 5×10^8 ions·cm^{-2}·s and for a maximum fluence not exceeding 10^{11} ions·cm^{-2}·s. Scanning tunneling microscopy (STM) images were recorded with a Nanoscope II STM from Digital Instruments, CA, USA. Time-of-flight (TOF) secondary ion mass spectrometry (SIMS) analysis was carried out on the samples before and after irradiation. Apart from trace carbon and oxygen, no impurities were detected, which includes Ni from the wire mesh and Ag from the irradiating ion.

X-ray topography measurements

The X-ray topographic (XRT) investigations of the Si surface [5], irradiated through the grid, so as to provide a grid shadow on the Si lattice is shown in Fig. 2. In XRT, a particular reciprocal lattice vector,

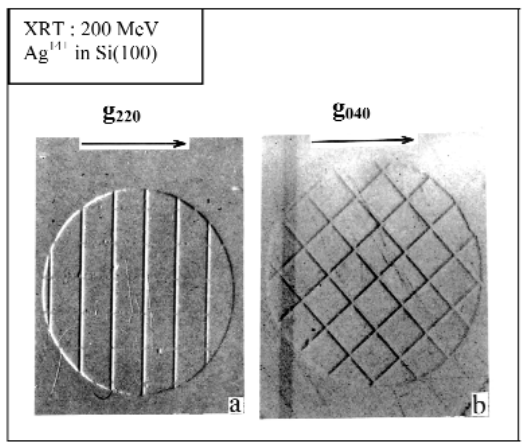

Fig. 2 X-ray topographic image of the irradiation interface. Both pictures are from the same sample taken with different reciprocal lattice vectors while doing topography. The irradiation interface is by design, created with one set of interface parallel to the [220] direction. Hence, in XRT, one set of lines are missing as $\mathbf{g_{220}}\cdot\mathbf{b} = 0$ for these while $\mathbf{g_{040}}\cdot\mathbf{b} \neq 0$ for any strain vector, **b**, generated.

g, is selected to perform X-ray diffraction according to the Bragg law, $2d\sin\theta = n\lambda$ or its equivalent form in terms of the wave vectors $\mathbf{K'} = \mathbf{K} + \mathbf{g}$, where $\mathbf{K'}$ and $\mathbf{K}$ are the diffracted and incident wave vectors, respectively. Wherever there is a strain gradient, the Bragg law is not satisfied, and a variation in intensity of the diffracted wave takes place, presenting a topography of the strain in the system under investigation.

The irradiation experiment of Fig. 2 was performed so that the shadow of the grid described earlier falls on the Si(100) surface, so that one set of grid lines (and hence their shadow) are parallel to the $\mathbf{g_{220}}$ of the crystal. Figure 2b shows the XRT of the Si(100) surface, employing the reciprocal lattice vector $\mathbf{g_{040}}$, demonstrating what is obtained. A replica of the grid has been imprinted onto the Si lattice. This replica represents the strain map at the edge of the irradiation interface, earlier described. The size of this replica does not change with the placement of the grid (5 mm–20 cm) in front of the Si(100) crystal, reflecting the highly parallel nature of ion beams employed.

The importance of this result comes through when $\mathbf{g_{220}}$ is employed to do the topography of the same Si(100) surface. This result is shown in Fig. 2a. One set of lines disappears, although the strain still exists. The reason for the absence lies in the fact that for this particular experiment, during irradiation, one set of grid lines was selected to align parallel to $\mathbf{g_{220}}$, as a result of which the strain vector **b** and the reciprocal lattice vector are perpendicular to each other during XRT providing for $\mathbf{g_{220}}\cdot\mathbf{b} = 0$. This selection rule results in no intensity in XRT. A few important points to note here are: (1) the strain appears at the irradiation interface only and does not appear in the body of the crystal under irradiation and (2) the strain is perpendicular to the irradiation interface.

The average surface density of Si is 10^{15} atoms·cm^{-2}, which makes our experiment a very dilute irradiation system, minimizing the possibility of interference between individual ion events. The range of the ions is calculated using the code TRIM [6] and found to be 21 μm. After irradiation, the surface of the crystal was treated with a Dash etchant to a depth of about 50 nm to remove surface contamination or damage. This procedure allows recording XRT and STM in air of the Si(100) surface with atomic resolution as reported in the literature [7,8]. It also allows us to present data from different depths inside the crystal. Etchings are made in stages to expose depths of 100–200 nm each time both for XRT recording and for the STM topography. STM was recorded to ascertain periodicity of the lattice after each etch.

Using XRT, we have developed a method to experimentally study this behavior [9]. It is seen that the boundary of the irradiation interface that gets imprinted in the silicon lattice owing to the mask shadow, changes with depth for Ag irradiation while remaining almost constant for Ti irradiation, for the range of depths investigated employing the etching procedure described above. As the mapped strain is directly proportional to the stress applied by the MeV ion, a stress map produced by the electronic energy loss is possible to sketch. This is shown schematically in Fig. 3. This result also corroborates the relationship between the strain generated in the lattice and the electronic energy loss suffered by the MeV ions.

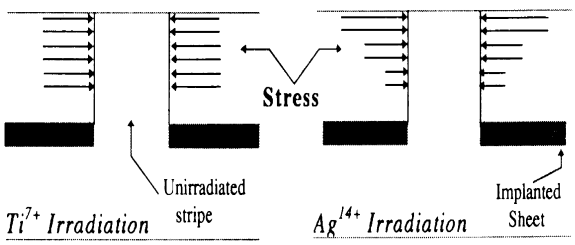

Fig. 3 Schematic representation of the stress distribution obtained from X-ray topography, inside the silicon lattice, after 100 MeV Ti^{7+} and 200 MeV Ag^{14+} irradiation.

RESULTS AND DISCUSSION

MeV ions are the best candidates for initiating an impulsive force, evidence of which is available in insulators and metallic glasses in the form of Coulomb explosion of atoms [10,11]. Following initial ionization, the incident ion energy is stored in the lattice as separation of charges. Relaxation takes place through an explosive mechanism, transferring the energy to lattice atoms in a time period smaller than the vibration period of the atoms, or inverse of the Debye frequency (~10–13 s).

It has been proposed that a single-crystalline lattice, in the presence of sufficient anisotropy, can support intrinsic localized modes (ILMs) [12], which has the possibility of transporting a large amount of energy through breather-like localized excitations [13]. These arise from the concept of solitary waves, first discovered in water, and arise due to excitation of many-body processes. It is mathematically described by the KdV equation [14]:

$$u_t + u_{xxx} + uu_x = 0, \text{ where } u = u(x,t) \tag{1}$$

is the height of the water wave at position x and time t, and the subscripts indicate partial differentiation. The second and third terms describe dispersion and nonlinearity, respectively.

Although established in a continuous media, solitons in a discrete lattice, also called lattice solitons or breathers, have been proposed and shown as waves traveling without dispersion along quasi 1-dimensional chains [13]. These are several lattice atoms, compacted, and hence store and carry substantial energy. The special property of these objects, carrying energy and momentum, arises from the process that produces them. Physically, an impulsive force, capable of producing nonlinear interatomic interactions, when suitably balanced by natural dispersion in a lattice, yields a traveling wave that proceeds without dispersion [15].

Energy supplied to a solid is stored in the linear chains of atoms as vibrational energy. It is well established that in the presence of a harmonic potential, the harmonic potential energy U^{harm} is given by

$$U^{\text{harm}} = \frac{k_2}{2}\sum_n (u_{n+1} - u_n)^2,$$

k_2 is the harmonic term and u_{n+1} and u_n are the displacements of the $(n + 1)$th and the nth atoms, respectively, from their equilibrium positions. Energy supplied to such a lattice is quickly distributed among all the lattice modes [16]. As a result, all atoms in the lattice perform oscillations, taking a share of the energy received. This well-known situation in lattice dynamics is presented in Fig. 4, as dispersion curves for a diatomic lattice containing masses m and M. The separation of frequency ω as a function

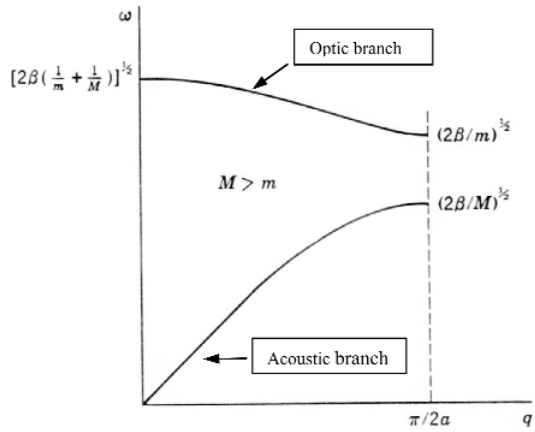

Fig. 4 Acoustic and optic branches of the frequency-vs.-wavenumber relation for a diatomic linear chain of atoms.

of the wave vector q into the acoustic and optic modes depends upon the relative in-phase and out-of-phase motion of the atoms within the unit cell.

But in the presence of an impulsive force, possible under certain conditions during the process of ion irradiation, the large amplitudes involved would naturally introduce anharmonic forces. What may thus happen can be qualitatively understood from Fig. 4. In the presence of an anharmonic potential, the vibrational frequencies would be quite unlike what is shown in the figure and hence will not follow any of the acoustic or optic branches. Such frequencies will be rejected by the lattice and could possibly be within the forbidden gap. Analytically, such values of frequency ω would lead to imaginary values for the wave vector q in the harmonic case of Fig. 4. But the energy received by the lattice through an impulsive force has to be stored all the same. This is only possible through localization of energy, which will allow for frequency of vibration of a few atoms, quite unlike anything that is supported by the optic and acoustic modes of Fig. 4. Such vibrational modes are called intrinsic localized modes (ILMs), where the term "intrinsic" is due to systems of study where anharmonicity is intrinsic (like some 1-dimensional materials).

In Fig. 5, we show a simulation of lattice vibrations of atoms that are connected by anharmonic forces, this time given by the potential energy form

$$U^{\text{anharm}} = \frac{k_2}{2}\sum_n (u_{n+1} - u_n)^2 + \frac{k_4}{4}\sum_n (u_{n+1} - u_n)^4,$$

where k_2 and k_4 are the harmonic and quartic anharmonic terms, while the other terms have similar meanings as before. A chain of 15 atoms is constructed to behave like a nonlinear lattice with periodic boundaries [17]. The vibrational evolution of the atoms start from the point marked at atom no. 8 and is calculated employing molecular dynamics. The time T_m is in units of a time period inherent to the system through the maximum harmonic plane wave frequency $\omega_m = 2\sqrt{(k_2/m)}$.

At $T_m = 0.0$, the lattice is cold when vibrational energy is supplied to atom no. 8. The evolution of this vibration takes place toward the left of this figure, as evident from atom configurations shown for various values of T_m. The localization of vibrational energy is immediately seen, comparing the situations for $T = 0.15\ T_m$ and $T = 15\ T_m$. While the atom no. 8 received the initial energy (stored as sum of kinetic and potential energies) as seen by the displacements of this atom and its neighboring atoms at $0.15\ T_m$, they have gone cold at $15\ T_m$, where the total energy of another set of atoms remains high. This would not have been the case in the event the atoms were connected by harmonic forces.

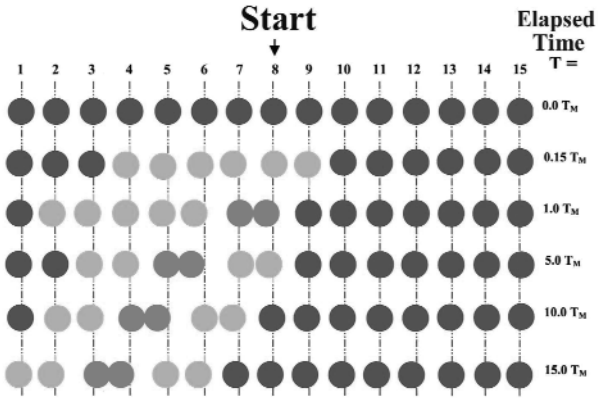

Fig. 5 Time evolution of vibrational energy in a 15-atom chain, interacting through anharmonic forces.

In order to see if the impulsive nature of MeV ion irradiation in the electronic loss regime does give rise to localization of vibrational energy that evolves in time, we tried to trap the energy at "irradiation interfaces" [5] that get defined in the shadow of the nickel grid described earlier. In the first experiment (EXPT1) we show STM data of the Si lattice after etching 50 nm of the surface of the sample, which corresponds to a calculated S_e of the ion at that depth to be 12 keV/nm. While the second experiment (EXPT2) is of the lattice from a depth of 10 μm with a reduced S_e = 8 keV/nm (see Fig. 1).

Several STM scans were performed on the Si lattice in the vicinity of the shadow of the nickel grid, spanning an area from the irradiated region into the shadow region of the grid. The result of one such scan from EXPT1 is shown in Fig. 6. Two distinct regions can be seen, consisting of (1) a perfectly periodic lattice on the right where the irradiation event took place and (2) a disordered region on the left, closer to the covered part of the Si crystal. This disordered region is 15 μm wide, after which a perfectly ordered reference Si surface is obtained. Thus, the disordered region can be called a transition region, between the irradiated lattice and the reference or unirradiated Si lattice. The disorder here is unique. Unlike point defects (obtained with low-energy irradiation), these do not anneal even at 1150 K. Moreover, our earlier X-ray topographic results [5] showed these contribute to a strain gradient perpendicular to the irradiation interface. Any implantation-induced disorder would not have shown such a strain gradient. The transition region cannot be shown here in full, as such an STM plot would lack atomic resolution.

However, a narrow transition region can be obtained. This is shown in Fig. 7, which represents STM scans from EXPT2 defined above. We now see three regions, namely, (1) the irradiated lattice/extension of the irradiated lattice in the near corner followed by (2) the transition region and (3) the reference region, protected under the grid. Inspection shows that the atomic rows of the irradiated lattice are parallel to those in the reference region. In the transition region, the rows are oriented by about 20º to those in the reference and irradiated regions. Careful examination shows that a small part in the center of the transition region still maintains the original orientation of the reference lattice structure.

To better understand the effects of the transition region, an STM scan of the misalignment of the rows seen in Fig. 7 is shown in Fig. 8 with higher magnification. The perfect arrangement of atoms in

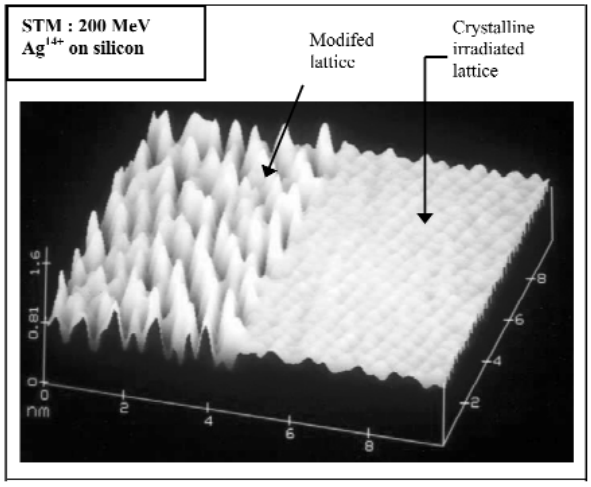

Fig. 6 The details of the irradiated lattice-transition region interface when the transition region is 15 μm wide, shown partly on the left. The transition region is marked by sharp structures showing termination of the irradiation front from the right. This surface layer is revealed by etching the irradiated Si(100) crystal by 50 nm (EXPT1, see text).

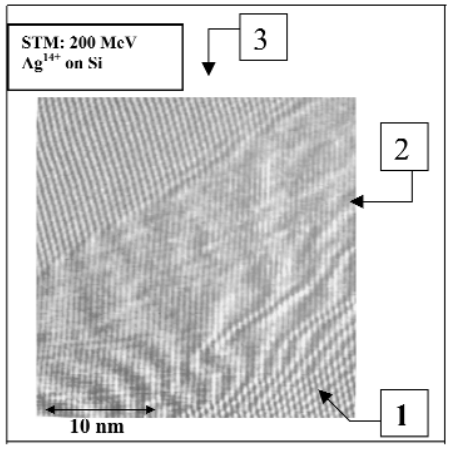

Fig. 7 STM scan of the Si(100) surface measuring 30 × 30 nm. The surface was achieved by etching the sample 10 μm (EXPT2, see text). Three regions are distinct as follows: irradiated lattice (near corner), transition region (middle), and reference region (far corner). The irradiation front in the near corner progresses a small distance inside the reference lattice producing a 10-nm-wide transition region.

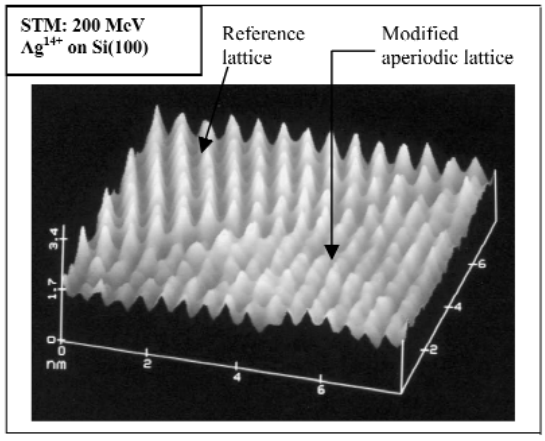

Fig. 8 An expanded view of Fig. 6 in the transition region-reference lattice interface showing details of atomic order in both. The transition region in the near corner is marked by lack of periodicity in one direction.

the far corner of this figure represents the reference lattice. The transition region is, however, characterized by an irregular arrangement of atoms showing piling up in some parts and depletion in others. In combination with Fig. 6, these results show that irradiation has not destroyed the regular structure of the lattice, but has created an increased disorder in the vicinity of the shadowed region.

The major difference in EXPT1 (S_e = 12 keV/nm) and EXPT2 (S_e = 8 keV/nm) arises from the electronic energy loss suffered by the ion, higher in the former. The differences show up in the form of a larger transition region in the former, as well as in the general ordering of atoms in this region. In EXPT1, the transition region is disordered completely compared to the original lattice directions [100] and [110], the disorder in EXPT2 is limited to within one single row of atoms, while periodicity is maintained in the orthogonal direction. This shows the scaling behavior of the imparted disorder in the Si lattice owing to electronic energy loss. The energy transfer to the interface takes place through the peri-

odic Si lattice, which is the most efficient pathway. For the irradiation interface, the greater extent of disorder near the surface shows a relationship to the initial energy loss. It is likely that an energy transfer to the lattice from an energy loss of 12 keV/nm would be larger than inside the crystal when it has reduced to 8 keV/nm. This, however, may not be linear. The energy transfer through the atomic chains are likewise to a greater extent (15 μm) and more disruptive, in the former. The extent of disruption is much reduced when the ion energy loss is 8 keV/nm at a depth of 10 μm, and this shows up as a disordered region of 10-nm width only, apart from retaining lattice periodicity in one direction.

The well-ordered atomic structure in the reference part is clear. The measured Si–Si lattice parameter is 0.54 nm. However, in the transition region the disorder is apparent. In this region, the Si–Si distances range from 0.22 to 0.58 nm. The localization of disorder in the transition region will cause the region to be strained, that is, compensated for by a counter strain in the surrounding material. We have verified and reported this effect. Employing XRT [5], we showed that under similar conditions of irradiation, the strain gradient existed only at the "irradiation interface", which is the same as the transition region denoted in our STM study.

Thus, we have shown here that following MeV ion irradation, impulsive forces introduce nonlinearity in the lattice, which results in the transport of energy from the irradiation site outwards in the form of vibrational energy. The STM data further show evidence for chains of atoms, which act as pathways or highways that allow such energy transport.

We further characterize the sharp structures in the transition region of EXPT1 by looking at their electronic properties, employing scanning tunneling spectroscopic measurements (STS). In STS, the presence of a tunnel current with positive (negative) sample voltage is associated with conduction band (valence band) states [18]. We plot the tunneling current (I) against the sample voltage (V) for two regions of the irradiated sample and compare the band-gaps obtained (width of the $I = 0$ region) with that of the reference Si(100). This is shown in Fig. 9. The following differences are noted: (1) the irradiated but ordered region (right-hand side of Fig. 6) has a band-gap of 1.2 eV (similar to reference Si) and an asymmetrically placed Fermi level (sample voltage $V = 0$), while the transition region (unirradiated, but modified) has a band-gap of 0.4 eV, and the Fermi level is symmetrically placed within the gap; and (b) a larger tunneling current for the latter [19]. These observations are conclusive evidence of

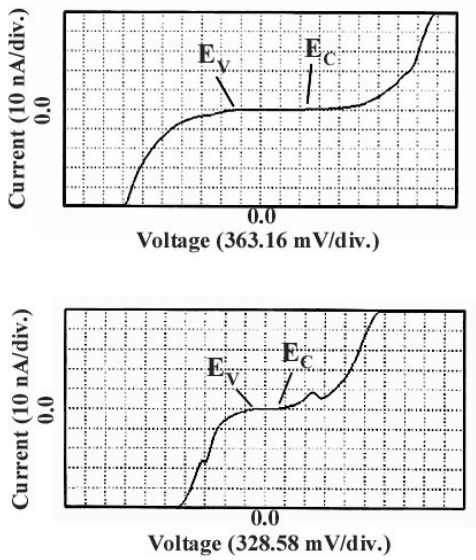

Fig. 9 Scanning tunneling spectroscopy (I-V plots) from (a) the irradiated but ordered region (right-hand side of Fig. 6) showing a band-gap of 1.2 eV (similar to reference Si) and (b) the transition region (unirradiated, but modified) showing band-gap of 0.4 eV.

modified electronic properties of the tip-like artificial structures at the transition region whose individual lateral dimension is 0.6 nm at the most. A striking gap of 0.4 eV for the sharp structures, selectively placed at the interface, is a result of local close packing of Si atoms, which gives an overall appearance of reduced atomic density in this region. The local close-packing also results in peaked electron densities and larger tunneling current (100 % increase for a tip-sample bias of 1.8 V). The placement of the Fermi level is possibly related to the local ordering of Si atoms. At the interface, lack of long-range order places the Fermi level at the center of the gap. While in the irradiated region, with anisotropy in interatomic lattice distances in the [100] and [110] directions, lead to the shifting of the Fermi level toward the valence band.

CONCLUSIONS

The transition region in EXPT1 consists of permanent subnanometer tips of Si whose band-gap and current emission capabilities have considerably modified due to a process initiated by the MeV ions. We have earlier stated that the transition region width scales with ion energy loss, from nanometers to several microns. With correct choice of opaque and transparent regions, it would be possible to cover an entire surface with uniform Si tips, or tips from any other material, provided they follow specific energy transport rules. It has been proposed here that a single-crystalline lattice, in the presence of sufficient anisotropy, can support ILMs, which have the possibility of transporting a large amount of energy through breather-like localized excitations. These arise from the concept of solitary waves, first discovered in water, and arise due to excitation of many-body processes.

ACKNOWLEDGMENT

We thank the accelerator staff at NSC, New Delhi, for assistance during the irradiation experiments.

REFERENCES

1. M. Levalois, P. Brogdanski, M. Toulemonde. *Nucl. Instrum. Methods B* **63**, 14 (1992).
2. V. S. Varichenko, A. M. Zaitsev, N. M. Kazutchits, A. R. Chelyadinskii, N. M. Penina, V. A. Martinovich, Y. Iatushko, W. R. Fahrner. *Nucl. Instrum. Methods B* **107**, 268 (1996).
3. S. Furuno, H. Otsu, K. Hojou, K. Izui. *Nucl. Instrum. Methods B* **107**, 223 (1996).
4. Z. G. Wang, Ch. Dufour, E. Paumier, M. Toulemonde. *J. Phys. Cond. Matter* **6**, 6733 (1994).
5. P. Sen, G. Aggarwal, U. Tiwari. *Phys. Rev. Lett.* **80**, 97 (1998).
6. N. Hayashi, R. Suzuki, M. Hasegawa, N. Kobayashi, S. Tanigawa, T. Mikado. *Phys. Rev. Lett*. **70**, 45 (1993).
7. G. S. Shekhawat, Ram P. Gupta, S. S. Shekhawat, D. P. Runthala, P. D. Vyas, P. Srivastava, S. Venkatesh, K. Mamhoud, K. B. Garg. *Appl. Phys. Lett.* **68**, 114 (1996).
8. Y. Nakagawa, A. Ishitani, T. Takahagi, H. Kuroda, H. Tokumoto, M. Ono, K. Kajimura. *J. Vac. Sci. Technol. A* **8**, 262 (1990).
9. Umesh Tiwari, Ph.D. thesis, Jawaharlal Nehru University, 1996.
10. S. Klaumunzer, M.-d. Hou, G. Schumacher. *Phys. Rev. Lett.* **57**, 850 (1986).
11. A. Audoard, J. Durai, M. Toulemond, A. Lovas, G. Szenes, L. Thome. *Phys. Rev. B* **54**, 15690 (1996).
12. A. J. Sievers and S. Takeno. *Phys. Rev. Lett.* **61**, 970 (1988).
13. P. Sen, J. Akhtar, F. M. Russell. *Europhys. Letters* **51**, 401 (2000).
14. G. Eilenberger. *Solitons,* Springer, Berlin (1983).
15. U. T. Schwarz, L. Q. English, A. J. Sievers. *Phys. Rev. Lett.* **83**, 223 (1999).
16. N. W. Ashcroft and N. David Mermin. *Solid State Physics*, Holt-Saunders, international ed., New York (1976).

17. A molecular dynamic simulation showing vibrational localization in a chain of monatomic lattice is available at the Web site http://www.lassp.cornell.edu/~sievers/ilm/
18. V. Ramachandran and R. M. Feenstra. *Phys. Rev. Lett*. **82**, 1000 (1999).
19. P. Sen and J. Akhtar. In *Microcrystalline and Nanocrystalline Semiconductors*, J. M. Buriak (Eds.), MRS Symposium Proceedings, Vol. 638, Pittsburgh, PA (2001).